CHAPTER 2

Mechanisms and Principles of 1D Self-Assembly of Peptides into β-Sheet Tapes

Robert P.W. Davies[1,2], **Amalia Aggeli**[1,2,*], **Neville Boden**[1,2], **Tom C.B. McLeish**[1,3], **Irena A. Nyrkova**[4], and **Alexander N. Semenov**[4]

Contents

[1] Centre for Self-Organising Molecular Systems, University of Leeds, Leeds LS2 9JT, United Kingdom
[2] School of Chemistry, University of Leeds, Leeds LS2 9JT, United Kingdom
[3] Department of Physics and Astronomy, University of Leeds, Leeds LS2 9JT, United Kingdom
[4] Institut Charles Sadron, Strasbourg Cedex, France

[*] Corresponding author.
E-mail address:a.aggeli@leeds.ac.uk

Advances in Chemical Engineering, Volume 35
ISSN 0065-2377, DOI: 10.1016/S0065-2377(08)00202-0

1. INTRODUCTION

Molecular self-assembly has attracted growing international research efforts and interest due to its central importance in biology and its role in the understanding of the molecular origin of a wide range of diseases (Burkoth et al., 1998; Lashuel et al., 2000; Yamada et al., 1998). With the onset of world-wide activities in nanoscale science and nanotechnology, molecular self-assembly has also provided inspiration for innovation (Wilson et al., 2002) and new product development in the fields of new nanostructured and biologically inspired materials, for example, for drug delivery, wound healing and tissue engineering, and novel processing routes (Collier et al., 2001; de Loos, 2001; Gronwald et al., 2002; Hanabusa et al., 1996; Marini et al., 2002; Qu et al., 2000; Terech and Weiss, 1997). Molecular self-assembly is an attractive route to nanostructured materials, which can have a number of key performance properties such as massive surface area and thus increased functional properties such as adsorption or binding. Nanomaterials can be light-weight and thus appropriate for miniaturization, they can be controllable, via external on/off triggering, and thus are injectable. Furthermore, molecular self-assembly is a spontaneous phenomenon, that is, thermodynamically driven; one implication is that self-assembling nanostructures are self-healing; they further provide a cheap, easy, and potentially fast methodology for bulk production of complex functional structures. The simple processes involved in the production of self-assembling structures using conventional techniques under mild conditions, without the need for expensive, sophisticated instruments, or harsh settings, are particularly suited to large-scale industrial applications.

Bioinspired protein-like self-assembly is one of the most fascinating and fast growing areas in molecular self-assembly. Proteins and peptides are the most versatile biological building blocks in nature in terms of chemistry, conformation, and functionality. They offer routes to sustainable, large-scale production since they can be produced not only by chemical means but also through genetic engineering. Another advantage is that they are environmentally friendly, "green" polymers. Also via precise control of the protein molecule, it is possible to exert precise control of the nanostructure, intermolecular interactions, binding, and (bio-)activity. One of the main drawbacks is that the immense chemical and conformational complexities make proteins difficult to understand quantitative and thus predict and control accurately and reliably.

In order to appreciate the fundamental physical and chemical principles that govern protein-like self-assembly, and thus learn how to exploit it, it is advantageous to start by using simple model peptide systems. Peptides can be easily synthesized in large numbers of systematic

variations to build structure–function relationships, they can be designed in order to minimize the chemical and conformational complexity of biological proteins, and they can evolve to progressively more complicated building blocks. Rationally designed peptides that self-assemble in 1-D into long β-sheet tapes offer one of the simplest and best understood systems to study hierarchical protein-like self-assembly (Aggeli et al., 1997a, b, 2001a, b, 2003a, b; Nyrkova et al., 2000a, b). The tapes are stabilized by precise intermolecular interactions, the aggregate structure is well-studied and unambiguously established, and the peptide building blocks offer versatility of the chemical and structural properties. Here we shall review the theoretical and experimental advances achieved so far in order to decipher the mechanisms and principles that describe and predict hierarchical β-tape self-assembly in a quantitative and reliable manner. We shall demonstrate these principles using predominantly the P_{11}-X family of rationally designed peptides. We shall summarize the conclusions of the studies with respect to the elucidation of the intrinsic self-assembling properties of the pure β-sheet structure, and the opportunities arising for functional peptide design.

2. MODEL OF HIERARCHICAL SELF-ASSEMBLING CHIRAL RODS IN SOLUTION

2.1. Theoretical rational of hierarchical self-assembling chiral rods in solution

A peptide in a β-strand conformation can be considered as a chiral rod-like unit, with complementary donor and acceptor groups aligned on opposing sides and having chemically different upper and lower surfaces (Figure 1a). This is a single step of coarse-graining from atomic detail to the nanoscale. The chiral unit is able to undergo 1D self-assembly in solution and to form the hierarchical structures in Figure 1 at concentrations depending on the values of a small set of coarse-grained interaction energies ε_j (Aggeli et al., 2001b; Nyrkova et al., 2000a, b; Weiss and Terech, 2006). An isolated monomer in solution will tend to be in a different conformation (Figure 1b), with lower free energy than in the rod-like state, giving rise to a conformational free energy change $\varepsilon_{\text{trans}}$.

The rod-like "monomers" self-assemble via multiple intermolecular interactions to form long twisted tapes (Figure 1c) with an association free energy change $\varepsilon_{\text{tape}}$ per intermonomer bond. The tape is chiral due to the chirality of the monomers, which gives rise to a left-handed twist around the long axis of the tape (Figure 1c). The differences in the chemical properties of the two faces of the tape give rise to a cylindrical curvature, causing

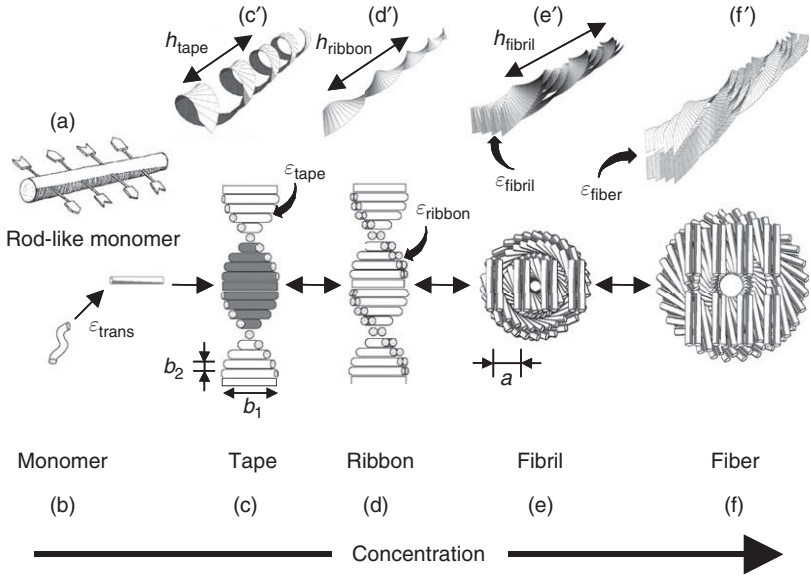

Figure 1 Model of hierarchical self-assembly of chiral rod-like monomer units (b): Local arrangements (c–f) and the corresponding global equilibrium conformations (c′–f′) for the hierarchical self-assembling structures formed in solutions of chiral molecules (a), which have complementary donor and acceptor groups, shown by arrows, via which they interact and align to form tapes (c). The black and the white surfaces of the rod (a) are reflected in the sides of the helical tape (c) which is chosen to curl toward the black side (c′). (e) and (f) show the front views of the edges of fibrils and fibers, respectively. Geometrical sizes for P_{11}-1 and P_{11}-2 peptides: inter-rod separation in a tape b_2 ($b_2 = 0.47$ nm); tape width, equal to the length of a rod, b_1 ($b_1 \approx 4$ nm); interribbon distance in the fibril, a ($a \approx 1.6$–2 nm for P_{11}-1, and $a \approx 2$–2.4 nm for P_{11}-2) (Aggeli et al., 2001b).

the tape to curl into a helical configuration (Figure 1c′), with helical pitch h_{tape} and radius r_{tape}:

$$h_{\text{tape}} = b_2\left(\frac{2\pi}{\gamma_\theta}\right)\left(1+\left(\frac{\gamma_\nu}{\gamma_\theta}\right)^2\right)^{-1} \tag{1}$$

$$r_{\text{tape}} = b_2\left(\frac{\gamma_\nu}{\gamma_\theta^2}\right)\left(1+\left(\frac{\gamma_\nu}{\gamma_\theta}\right)^2\right)^{-1} \tag{2}$$

where γ_ν and γ_θ are the tape bend and twist angles (in radians) per monomer rod along the tape and b_2 is the distance between adjacent rods in the tape.

One face of the tape is expected to be less soluble than the other (i.e., black is more hydrophobic if the solvent is water in Figure 1c). This difference results in intertape attraction and hence in double-tape (ribbon, Figure 1d)

formation, with an associated energy $\varepsilon^{\text{attr}}_{\text{ribbon}}$ per peptide. Both faces of the ribbon are identical (white in Figure 1d) and are characterized by a saddle curvature. Hence, the ribbon does not bend, and its axis is straight at equilibrium (Figure 1d′). The white sides of the ribbons can also be mutually attractive with an associated energy $\varepsilon^{\text{attr}}_{\text{fibril}}$ per pair of interacting peptides, leading to stacking of ribbons into fibrils (Figure 1e). Furthermore, the ends of the rods at the edges of the fibrils can also be mutually attractive, causing fibrils to entwine into fibers (Figure 1f), stabilized by attraction energy $\varepsilon^{\text{attr}}_{\text{fiber}}$.

The whole set of the self-assembling structures in Figure 1 are left-handed twisted due to the chirality of the monomer. If the ribbons were not twisted, an unlimited growth of stacks of them would be expected. Instead, when twisted ribbons aggregate into stacks, fibrils with well-defined widths are formed. Fibers are formed in a similar way from twisted fibrils, but again to well-defined widths. In order to aggregate, twisted objects must bend and adjust their twist in response to the packing constraints imposed by its twisted neighbors. Hence, there is an elastic energy cost $\varepsilon_{\text{elast}}$, which must be compensated for, by the gain in attraction energy (coming from $\varepsilon^{\text{attr}}_{\text{ribbon}}$, $\varepsilon^{\text{attr}}_{\text{fibril}}$, and $\varepsilon^{\text{attr}}_{\text{fiber}}$) upon stacking. The distortion energy $\varepsilon_{\text{elast}}$ is higher for thicker stacks. This serves to stabilize the widths of fibrils and fibers. Thus, the fibril width is determined by a balance between the gain in attraction energy (coming from $\varepsilon^{\text{attr}}_{\text{fibril}}$) associated with ribbon stacking, and the elastic cost on the ribbons associated with fibril formation. If the ribbon contour length is fixed and the deformations are weak, from symmetry arguments we find that this cost is

$$\varepsilon_{\text{elast}} = \frac{1}{2} k_{\text{bend}} (\nu - \nu_0)^2 + \frac{1}{2} k_{\text{twist}} (\theta - \theta_0)^2 \tag{3}$$

per unit length of each ribbon in the fibril, where ν and θ are the local curvature and the local twist strength of the ribbon within a fibril, $\theta_0 = 2\pi / h_{\text{ribbon}}$ is the equilibrium value of twist strength of an isolated ribbon, while its bend strength is zero ($\nu_0 = 0$), and k_{bend} and k_{twist} are the ribbon elastic constants (Nyrkova et al., 2000a, b). For a ribbon at a distance ρ from the central axis of a fibril, it can be shown that $\nu = \gamma^2 \rho / (1 + \gamma^2 \rho^2)$ and $\theta = \gamma / (1 + \gamma^2 \rho^2)$, where $\gamma = 2\pi / h_{\text{fibril}}$ (h_{fibril} is the fibril's helical pitch). The thicker the fibril is, the larger the typical ρ are, and hence the higher the cost $\varepsilon_{\text{elast}}$. Thus, the net energy gain $\varepsilon_{\text{fibril}}$ per peptide in a fibril

$$\varepsilon_{\text{fibril}} = \frac{p - 1}{2p} \varepsilon^{\text{attr}}_{\text{fibril}} - \varepsilon^{\text{elast}}_{\text{fibril}} \tag{4}$$

has a maximum at some p (p is the number of ribbons in the fibril). Hence, a well-defined width of fibrils arises, corresponding to this optimal p.

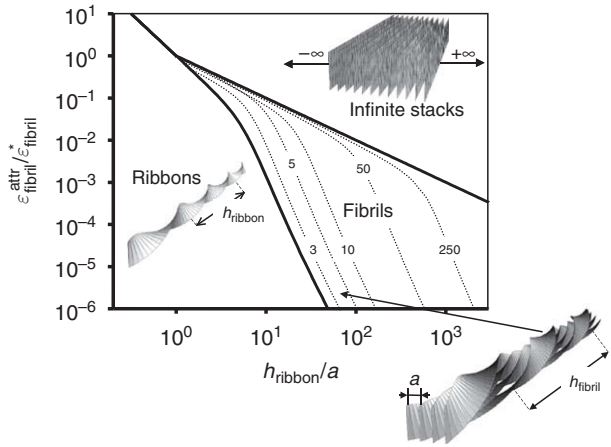

Figure 2 Phase diagram of a solution of twisted ribbons which form fibrils, where the relative helix pitch of isolated ribbons h_{ribbom}/a is plotted against the relative side-by-side attraction energy between ribbons $\varepsilon^{attr}_{fibril}/\varepsilon^{*}_{fibril}(\varepsilon^{*}_{fibril} \equiv (2\pi^2 b_2/a^2)k_{twist})$. The areas divided by the thick lines reveal the conditions where ribbons, fibrils, and infinite stacks of completely untwisted ribbons are stable. The dotted lines are lines of stability for fibrils containing p ribbons (p are written on the lines); $k_{bend}/k_{twist} = 0.1$ (Aggeli et al., 2001b).

The diagram of possible aggregate structures calculated by using this model, and seeking its structure of minimum free energy in each case, is shown in Figure 2. Fibrils with finite diameter are seen to be stable for a wide range of values of $\varepsilon^{attr}_{fibril}$ provided that the intrinsic pitch h_{ribbon} of the lone ribbon strongly exceeds the interribbon gap, a, in the fibril. For low $\varepsilon^{attr}_{fibril}$, the ribbons do not stack into fibrils. For high $\varepsilon^{attr}_{fibril}$, the ribbons form infinite aggregates (sheet-like crystallites) in which the ribbons are completely untwisted. The optimum number p of stacked ribbons per fibril, and hence the fibril diameter, increases with h_{ribbon} and $\varepsilon^{attr}_{fibril}$. This is usually accompanied by an increase in h_{fibril}.

The concentration ranges over which the various self-assembled structures are observable, their contour lengths, and abruptness of interstructure transformations with concentration are determined by the energy parameters ε_j. For example, if ε_{trans} is high enough ($\varepsilon_{trans} > 4$, all energies here are measured in k_BT units) and ε_{ribbon} is small (≤ 1), the single tapes emerge abruptly at

$$c^{tape}_{cr} \cong \nu^{-1}_{tape} \exp(-\varepsilon_{tape} + \varepsilon_{trans}) \tag{5}$$

and their typical aggregation number is

$$\langle m_{tape} \rangle \cong \left[\left(\frac{c}{c^{tape}_{cr}} \right) - 1 \right]^{\frac{1}{2}} \exp\left(\frac{\varepsilon_{trans}}{2} \right) \tag{6}$$

if $c_{cr}^{tape} < c < c_{cr}^{ribbon}$ (c is the total peptide concentration and ν_{tape} is the "freedom" volume of the bonds forming the tape). Next, given the tape bend and twist are not very high, that is, ε_{elast} (cf. Equation (3)) is small enough, the net ribbon energy

$$\varepsilon_{ribbon} = \frac{1}{2}\varepsilon_{ribbon}^{attr} - \varepsilon_{ribbon}^{elast} \tag{7}$$

is positive. Hence, at concentration

$$c_{cr}^{ribbon} \cong c_{cr}^{tape} + c_{tape}^{max}, \qquad c_{tape}^{max} \cong \nu_{tape}^{-1}\varepsilon_{ribbon}^{-2}\exp(-\varepsilon_{tape}) \tag{8}$$

the ribbons emerge; above c_{cr}^{ribbon}, the population of peptide in single tapes saturates at c_{tape}^{max} and all extra peptide goes into ribbons; simultaneously the average aggregation number of ribbons grows as

$$\langle m_{ribbon}\rangle \approx \left[\left(\frac{c}{c_{cr}^{ribbon}}\right) - 1\right]^{\frac{1}{2}} \varepsilon_{ribbon}^{2} \exp\left(\frac{\varepsilon_{trans} + \varepsilon_{tape}}{2}\right) \tag{9}$$

whereas the length of tapes saturates at

$$\langle m_{tape}\rangle \cong \varepsilon_{ribbon}^{-1} \tag{10}$$

The formulae (Equations (5), (6), (8)–(10)) are asymptotic. To realize sequentially the entire hierarchy of structures in Figure 1, with increasing monomer concentration, it is essential that $\varepsilon_{tape} >> k_B T >> \varepsilon_{ribbon} >> \varepsilon_{fibril} >> \varepsilon_{fiber}$, otherwise, some structures may not appear. These are the net energies gained per one peptide inside the corresponding structures as compared to a peptide inside the structure of the previous level.

2.2. Experimental evidence of hierarchical peptide self-assembly in solution

2.2.1. Tape-forming peptides

Peptide P_{11}-1 ($CH_3COQQRQQQQQEQQNH_2$) has been designed de novo with a sequence of glutamine (Q, Gln) residues, whose side chains are believed to interact strongly in water (Perutz et al., 1994) via hydrophobic and complementary hydrogen-bonding interactions. Arginine (R, Arg) and glutamate (E, Glu) residues were placed in positions 3 and 9 to provide molecular recognition between adjacent antiparrallel β-strand peptides in tape-like aggregates and to prevent random peptide association. These favorable intermolecular side-chain interactions, together

with the cooperative intermolecular hydrogen bonding between peptide backbones, will result in high scission energy $\varepsilon_{\text{tape}}$, thus promoting β-sheet tape formation (Figure 1c). One side ("black") of the tape will be lined by the $CONH_2$ groups of the Gln residues, whilst its other side ("white") will be lined by Gln, Arg, and Glu. At low pH, there will also be a net positive charge per peptide; thus the high hydrophilicity of both surfaces of the tape, combined with the electrostatic repulsion between positively charged surfaces, will result in very small $\varepsilon^{\text{attr}}_{\text{ribbon}}$ and $\varepsilon^{\text{attr}}_{\text{fibril}}$ energies compared to k_BT, thus promoting predominantly single tape formation for low enough peptide concentration in acidic solutions.

Solutions of P_{11}-1 at very low concentrations are found to consist predominantly of monomeric random coil conformation (Figures 1b and 3a), whereas at higher concentrations $c \geq 0.01$ mM, they contain semiflexible tapes with a width $W \approx 4$ nm, equal to the expected length of an 11-residue peptide in a β-strand conformation, and persistence length $\tilde{l} < 0.3$ μm. The different chemical nature of the two sides of the tape seems to cause it to bend and twist simultaneously, resulting in curly tapes with a left-handed twist, a helical pitch $h_{\text{tape}} \approx (30 \pm 15)$ nm, and a radius $r_{\text{tape}} \approx 5$ nm. At $c \geq 1$ mM, loose ribbons are also observed, with $\tilde{l} \sim 0.3 - 1$ μm and $h_{\text{ribbon}} \approx (50 \pm 20)$ nm. These experimental data were treated with the theoretical model in order to derive the magnitudes of the bend $\gamma_\nu = 3°$ and twist $\gamma_\theta = 3°$ angles for the single tapes and the ribbons (Table 1).

Aqueous solutions of P_{11}-1 tapes produce FTIR spectra with absorption maxima in amide I′ at 1,630 and 1,690 cm^{-1}, demonstrative of a predominantly antiparallel β-sheet structure. They also exhibit characteristic β-sheet

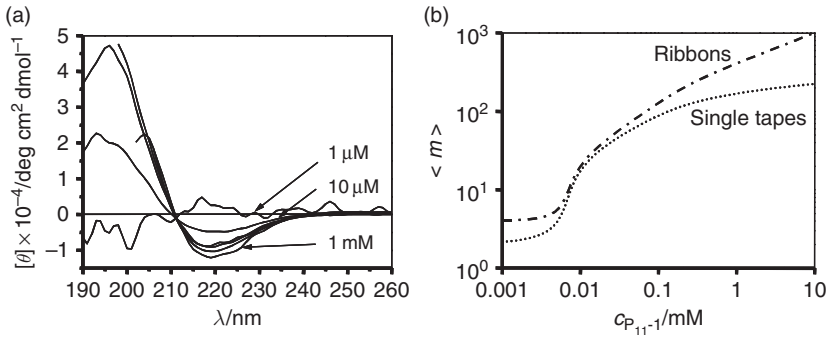

Figure 3 Self-assembling properties of P_{11}-1. (a) Far-UV CD spectra as a function of peptide concentration in water at pH = 2. (b) Theoretical concentration dependence of the average number $\langle m \rangle$ of peptides per single tape (dotted line) and in ribbons (dash-dot line). Minimum number of peptides in tapes is two and in ribbons is four. The predicted lengths of tapes and ribbons are in agreement with the observed lengths in the TEM pictures for the same peptide concentration (Aggeli et al., 2001b).

Table 1 Magnitudes of molecular parameters and macroscopic properties of the aqueous solutions of the two de novo-designed self-assembling β-tape forming peptides P_{11}-1 and P_{11}-2 (Aggeli et al., 2001b)

	P_{11}-1			P_{11}-2		
	β-Tapes	Ribbons	Fibrils	β-Tapes	Ribbons	Fibrils
$c_{cr}/\mu M$	8	1,000	$c > 25{,}000$	<90	90	700 ± 200
ε_{trans}/k_BT	6.5 ± 1.5			3 ± 1		
ε_{tape}/k_BT	31.0 ± 1.5			24.5 ± 1.0		
$\varepsilon_{ribbon}/k_BT$		$(3.5 \pm 1.5)10^{-3}$			0.6 ± 0.3	
$\varepsilon_{fibril}/k_BT$			$<10^{-3}$			$(2.0 \pm 0.3)10^{-4}$
Pitch h/nm	30 ± 15	50 ± 20			160 ± 40	160 ± 40
Twist angle $\gamma_\theta/^o$	3	3		1	1	1
Bend angle $\gamma_\upsilon/^o$	3	0			0	0
$\tilde{l}/\mu m$	<0.3	0.6 ± 0.2			1.0 ± 0.3	20–70
$L/\mu m$,($c = 6$ mM)	10^{-1}	10^{-1}–10^{0}		10^{-3}	10^{0}	10^{17}
Properties of aqueous solution	Isotropic fluid ($c < 13$ mM) Nematic fluid/gel ($c > 13$ mM)			Isotropic fluid ($c < 0.9$ mM) Nematic fluid ($c \approx 0.9$–6 mM) Nematic gel ($c > 6$ mM)		

CD spectra (Manning et al., 1988) with minimum and maximum ellipticities at 218 nm and 195 nm, respectively (Figure 3a). The fraction of the peptide in β-sheet tapes starts to grow abruptly at a critical concentration $c_{cr}^{tape} \approx 0.008$ mM. The two-state transition from random coil to β-sheet with increasing concentration has an isodichroic point at 211 nm (Figure 3a). ε_{trans} and ε_{tape} were treated as fitting parameters and it was thus possible to describe well the growth of the β-sheet CD band with concentration. The best-fit energy values obtained are in Table 1. The ε_{trans} energy results in the nucleated growth of tapes, manifested by a "sudden" onset of β-sheet tape formation at c_{cr}^{tape}. By using these values of energetic parameters, this single tape model predicts a mean tape contour length for a given peptide concentration, which agrees well with the observed range of contour lengths in the TEM images for the same concentration. At $c_{cr}^{ribbon} \approx 1$ mM, loose ribbons start appearing, implying a weak attraction between tapes. This attraction may be mediated by multiple, cooperative, complementary hydrogen bonding and van der Waals interactions between the —$CONH_2$ groups of glutamine side chains, which line completely one of the two polar sides of the tapes. From the value of c_{cr}^{ribbon}, it can be estimated that the ribbons are stabilized by $\varepsilon_{ribbon} = (0.0035 \pm 0.0015)\ k_BT$. Fibrils (Figure 1e′) are not observed up to $c = 25$ mM, hence using the theoretical model, it can be estimated that $\varepsilon_{fibril} < 10^{-3}\ k_BT$ and $\varepsilon_{fibril}^{attr} \leq 0.1\ k_BT$.

2.2.2. Fibril-forming peptides

How can a tape-forming peptide be modified in a rational manner so that it becomes a fibril-forming peptide at μM–mM concentration? According to the theoretical model, in order to design a peptide with an increased tendency to associate into ribbons, the magnitude of ε_{ribbon} must be increased either by decreasing $\varepsilon_{ribbon}^{elast}$or by increasing $\varepsilon_{ribbon}^{attr}$. The latter can be achieved by addition of salts or of appropriate cosolvents, or by changing the peptide primary structure. In particular, glutamines at positions 4, 6, and 8 of P_{11}-1 were replaced by phenylalanine, tryptophan, and phenylalanine, respectively. This new peptide, P_{11}-2 (CH_3CO—QQRFQWQFEQQ—NH_2), will form β-sheet tapes with a hydrophobic "adhesive" stripe running along one side of the tape, which will promote their association into ribbons in water. At $c \geq 0.1$ mM in water, P_{11}-2 is found to form long, stable semiflexible β-sheet ribbons with a width of 2–4 nm, which fits with the expected cross section of $\approx 2 \times 4\ nm^2$ of these ribbons and a persistence length $\tilde{l} \approx 1$ μm (Figure 4a). At $c \geq 0.6$ mM, a second transition from ribbons to fairly rigid fibrils is observed (Figure 4b and c). The fibrils have a well-defined screw-like structure with typical minimum and maximum widths $W_1 \approx 4$ nm and $W_2 \approx 8$ nm, respectively. At even higher concentrations still, a third structural transition takes place and fibers are detected,

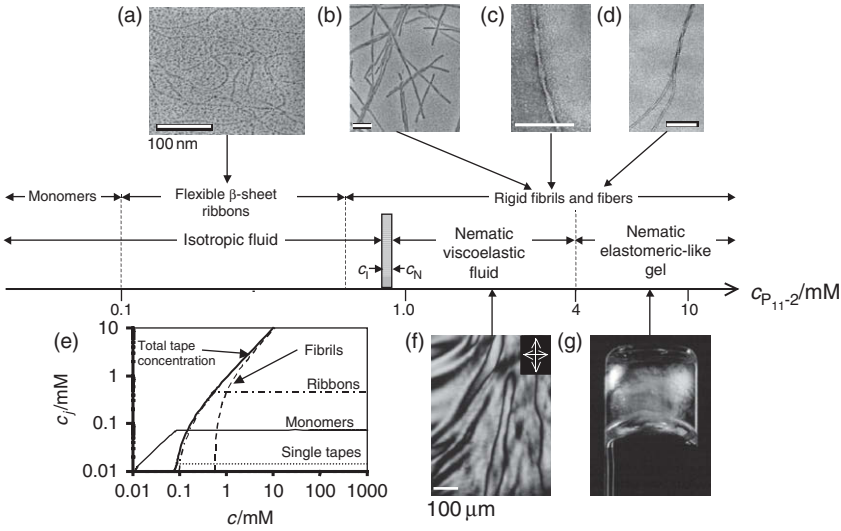

Figure 4 Self-assembling structures and liquid crystalline phase behavior observed in solutions of P_{11}-2 in water with increasing peptide concentration c (log scale). Electron micrographs (a) of ribbons ($c = 0.2$ mM), (b) and (c) of fibrils ($c = 6.2$ mM), and (d) fibers. The curves in (e) were calculated with the generalized model described in the text (see also Figure 5d). The polarizing optical micrograph (f) shows the thick thread-like texture observed for a solution with $c = 3.7$ mM in a 0.2 mM pathlength microslide; (g) shows a self-supporting birefringent gel ($c = 6.2$ mM) in an inverted 10 mM o.d. glass tube, viewed between crossed polarizers. The scale bars in (a–d) correspond to 100 nm, in (f) to 100 µm (Aggeli et al., 2001b).

typically comprised of two entwined fibrils (Figure 4d). The sequence of these structural transitions is also supported by distinctive far- and near-UV CD spectra, corresponding to P_{11}-2 monomers, ribbons, and fibrils (Figure 5a and b).

P_{11}-2 is predominantly in the monomeric random coil conformation at low concentrations (Figure 1b), whereas the fraction of peptide in β-sheet structures starts to grow abruptly at $c \approx 0.07$ mM (Figure 5a and c). Assuming only the presence of tapes in the experimental solutions, ε_{trans} and ε_{tape}, were treated as fitting parameters, it was possible to describe well the experimentally observed β-sheet growth with concentration. However, this single tape model yields a mean tape length of about 20 nm at $c = 0.2$ mM (Figure 5d), much shorter than the observed length $\geq$500 nm (Figure 4a). It is possible, however, to describe the experimentally observed growth of aggregate (solid line in Figure 5c) and simultaneously to predict the occurrence of these long aggregates (Figure 4a) by assuming the presence of tapes and ribbons in the solution. In this way, the experimental data was fitted with three parameters: ε_{trans}, ε_{tape}, and ε_{ribbon} (Figure 1d).

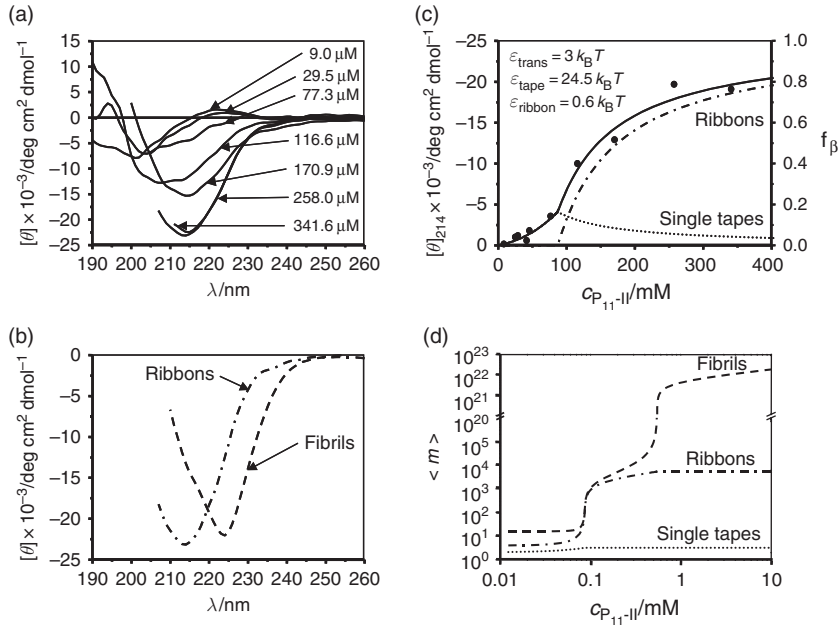

Figure 5 Self-assembling behavior of P_{11}-2. (a) and (b) Far-UV CD spectra in water at 20° C. (b) Comparison of the CD spectra of isotropic solutions of P_{11}-2 ribbons and of fibrils at $c = 0.3$ mM. The fibril spectrum reveals a red-shifted negative band (centered at 224 nm, compared to 214 nm for ribbons), possibly arising from the superposition of a strong aromatic CD band on the classical β-sheet CD spectrum. (c) Fit of the theoretical model (solid line) for the self-assembly of peptides into single and double β-sheet tapes, to the measured concentration dependence of the mean residue ellipticity $[\theta]$ of the negative CD band at $\lambda = 214$ nm. $[\theta]_{214}$ is taken to be a linear function of the fraction f_β of peptides in β-sheet tapes. The fractions of peptides involved in single and double tapes are represented with dotted and dash-dot lines, respectively. (d) Theoretical concentration dependencies of the average number $\langle m \rangle$ of peptides in single tapes (dotted line) and in ribbons (dash-dot line) and in fibrils made of $p = 4$ ribbons (dashed line). The molecular parameters were chosen to comply with the fit (c) and with the observed lengths of ribbons at $c = 0.2$ mM and with the transition concentration from ribbon to fibrils at $c = 0.6$ mM. Note that the minimum number of peptides in tapes is two, in ribbons is four, and in fibrils is eight (Aggeli et al., 2001b).

These long aggregates then turn out to be double tapes (ribbons) rather than single ones (Figure 5c and d). The CD spectra as a function of concentration have no isodichroic point (Figure 5a), further supporting that more than two states, that is, peptide monomers, β-tapes, and ribbons, are involved in the conformational transition. The best-fit energy values obtained are $\varepsilon_{trans} = (3 \pm 1)\ k_BT$, $\varepsilon_{tape} = (24.5 \pm 1.0)\ k_BT$, and $\varepsilon_{ribbon} = (0.6 \pm 0.3)\ k_BT$.

The estimated ε_{trans} is higher for P_{11}-1 than for P_{11}-2 (Table 1). Although both peptides have the same length, they may have different propensity to form a random coil and a β-strand, which may account for this difference in ε_{trans}. In particular P_{11}-1 has less bulky side-groups, hence it is generally more flexible than P_{11}-2, and as a result P_{11}-1 should have higher entropy in the coiled conformation. The magnitude of ε_{tape} is also higher for P_{11}-1 than for P_{11}-2, which indicates that the intermolecular glutamine side-chain interactions between P_{11}-1 peptides are more efficient at promoting self-assembly compared to intermolecular aromatic side-chain interactions between P_{11}-2 peptides. ε_{ribbon} is at least two orders of magnitude lower for P_{11}-1 compared to P_{11}-2, as engineered by peptide design. This difference explains the shorter (by one order of magnitude) length of P_{11}-1 ribbons compared to P_{11}-2 ones (Table 1). It also accounts for the one order of magnitude difference in critical concentrations for ribbon formation between the two peptides. This results in stabilization of single, curly β-tapes in a wide range of P_{11}-1 concentrations. In contrast, P_{11}-2 tapes are not observed because they convert to ribbons as soon as they are 3–4 peptides long, at very low concentration.

The formation of fibrils (Figure 4b) at higher concentrations of P_{11}-2 implies the presence of a weaker attraction between the polar sides of P_{11}-2 ribbons ($\varepsilon^{attr}_{fibril}$, Figure 1e′). From the concentration at which fibrils appear, we calculate $\varepsilon_{fibril} = (2.0 \pm 0.3) \cdot 10^{-4}\ k_B T$. Despite this attraction, the fibril dispersions are stable and the fibril diameter is finite (rather than growing indefinitely). Furthermore, the fibril width W_1 corresponds to the expected length of an 11-residue β-strand, whilst W_2 corresponds to roughly the thickness of 4 ribbons (i.e., 8 single tapes, each tape with a thickness of ca 1 nm) per fibril and is concentration independent (at least from 0.6 to 7 mM). The energy required to break such a fibril, scission energy ε_{sc}, is $\varepsilon_{sc} = 8\varepsilon_{tape} \sim 200\ k_B T$ (comparable to covalent bond energies!) and is much higher than that of a single ribbon $\varepsilon_{sc} = 2\varepsilon_{tape} \sim 50\ k_B T$. This results in fibrils of extraordinary predicted equilibrium average length: $L_{fibril} \sim 10^8$ km!, compared to $L_{ribbon} \sim 1$ μm, for $c = 6$ mM.

2.2.3. Effect of chirality

The formation of fibrils can be explained by the theoretical model of stabilization by twist. β-Sheet ribbons have an intrinsic left-handed twist, due to the L-chirality of peptides (Chothia, 1973). The fibrils also exhibit a left-handed twist with a twist pitch h_{fibril} of approximately 120–200 nm (Figure 4c). Based on the observed geometrical characteristics of P_{11}-2 ribbons and fibrils in combination with the theoretical model, the following parameters can be estimated: $h_{ribbon} \sim 120$–200 nm, elastic constants k_{bend} and k_{twist}, and twist angle $\gamma_\theta = 1°$ for isolated P_{11}-2 ribbons, and $\varepsilon^{attr}_{fibril} \sim 0.015\ k_B T$ for fibrils (Table 1). The magnitude of $\varepsilon^{attr}_{fibril}$ is expected to be similar both for P_{11}-1 and P_{11}-2, because of the identity of their polar

sides. However, P_{11}-1 ribbons are three times more twisted than P_{11}-2 ones (twist angles γ_θ in Table 1). The higher elastic penalty $\varepsilon_{\text{fibril}}^{\text{elast}}$ associated with untwisting P_{11}-1 ribbons compared to P_{11}-2 ones seems to result in lower overall magnitude of $\varepsilon_{\text{fibril}}$ for P_{11}-1 compared to P_{11}-2 and thus prevents the stacking of P_{11}-1 ribbons into fibrils. This may explain why P_{11}-1 ribbons do not combine into fibrils up to $c = 25$ mM, whilst P_{11}-2 ribbons form fibrils at $c < 1$ mM.

2.2.4. Nematic fluids and gels

The fibrils and fibers are rigid and thus they give rise to the formation of a nematic phase at $c \geq 0.9$ mM (0.001 v/v) for P_{11}-2. The texture in the optical micrograph (Figure 4f) and its dependence on flow is characteristic of viscoelastic nematic fluids (Figure 6a) of semirigid polymers (Dobb et al., 1977). The isotropic-to-nematic phase separation gap is narrow: $0.8\,\text{mM} < c_I < c_N < 0.9$ mM (relative gap width $w \equiv c_N/c_I - 1 < 0.13$) and is insensitive to temperature variations up to at least 60° C. Polydisperse rigid-rod solutions have much wider phase separation gaps ($w \sim 2$) (Semenov and Khokhlov, 1988). The fibrils behave more like typical semirigid (worm-like) chains with hard-core excluded volume interactions, for which $w \sim 0.09$ (Semenov and Khokhlov, 1988). The isotropic-to-nematic transition of such chains with rectangular cross section $W_1 \times W_2$ is predicted (Semenov and Khokhlov, 1988) to occur at volume fractions $\Phi_{IN} \approx 5.5W/\tilde{l}_{\text{fibril}}$ [where $W \approx 2W_1W_2/(W_1 + W_2)$, provided that $L \geq \tilde{l}_{\text{fibril}}$]; this yields for P_{11}-2, $\Phi_{IN} \approx 0.0004 - 0.0015$ v/v (corresponding to $c_{IN} \approx 0.4$–1.5 mM), in agreement with our observations. $\tilde{l}_{\text{ribbon}}$ for P_{11}-1 is one to two orders of magnitude shorter than $\tilde{l}_{\text{fibril}}$ of P_{11}-2. The isotropic-to-nematic transition of solutions of such semiflexible ribbons of P_{11}-1 is predicted to occur at $\Phi_{IN} \approx 0.015$–0.05 v/v (corresponding to 15–50 mM). Indeed, it is found that P_{11}-1 forms nematic phase at $c \sim 13$ mM (Table 1).

At $c \geq 4$ mM, the birefringent solution of P_{11}-2 becomes a self-supporting birefringent gel (Figure 4g). Gelation is associated with onset of fiber

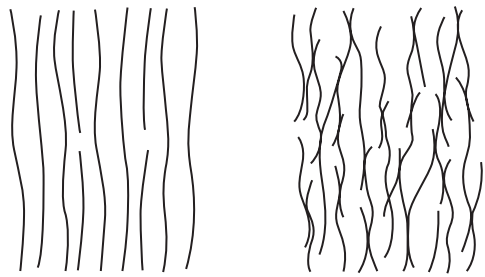

Figure 6 Schematic diagram showing arrangement of fibrils in nematic fluids (a) and the fiber-like junctions in nematic gel states (b) (Aggeli et al., 2003a, b).

formation (Figure 4) which leads to the perception that in the gels, fibrils are linked by fiber-like junctions (Figure 6b). In contrast, tape-based gels are more extendable (Aggeli et al., 1997a, b) and relax slowly with time, behavior indicative of transient gels of semiflexible polymers. It can be concluded that the type of polymer (tape, ribbon, or fibril, each associated with its own characteristic flexibility, contour length and crosslinking mechanism) determines the liquid crystalline and gelation properties of its solution.

3. RESPONSIVENESS TO EXTERNAL TRIGGERS

The magnitudes of energetic parameters that govern and quantify peptide self-assembly and material properties are dependant on a number of variables such as solution conditions (e.g., pH, ionic strength, and relative dielectric constant) and molecular/chemical permutations (e.g., peptide length and amino acid composition). Appropriate choice of solution conditions in combination with rational peptide design allow the control of a number of crucial properties, for example, the magnitudes of critical concentrations for self-assembly of particular types of aggregate, the number of each type of aggregate present and their average length as a function of peptide concentration, the engineering of responsiveness of the self-assembling peptides to a wide range of external triggers, the lifetime and dissolution rate of the aggregates and the material (mechanical, nematic, and gelation) properties.

3.1. pH

A series of systematically varied peptides have been previously designed and studied in order to illustrate that it is possible to engineer responsiveness of self-assembling peptide materials to external chemical triggers (Aggeli et al., 2003a, b). Solutions of P_{11}-2 peptide form stable gels below pH 5, where only arginine is positively charged and the total net charge is +1 per peptide. Above pH 5, the net charge is 0, hence flocculation of the peptide occurs. Thus, it becomes apparent that stabilization of fibrillar dispersions requires a net positive or negative charge per peptide molecule. Incorporation of further charged groups in the primary structure of P_{11}-2 molecule, such as Glu (—CH_2CH_2COOH) or Orn (—$CH_2CH_2CH_2NH_2$), enables self-assembly to be rapidly (seconds) and reversibly controlled by simply changing pH.

This is demonstrated by the behavior of two peptide variants: P_{11}-4 (CH_3CO—QQRFEWEFEQQ—NH_2), which can be switched from its nematic to its isotropic fluid state by increasing pH, and P_{11}-5 (CH_3CO—QQOFOWOFQQQ—NH_2) (O = ornithine), designed to exhibit the opposite

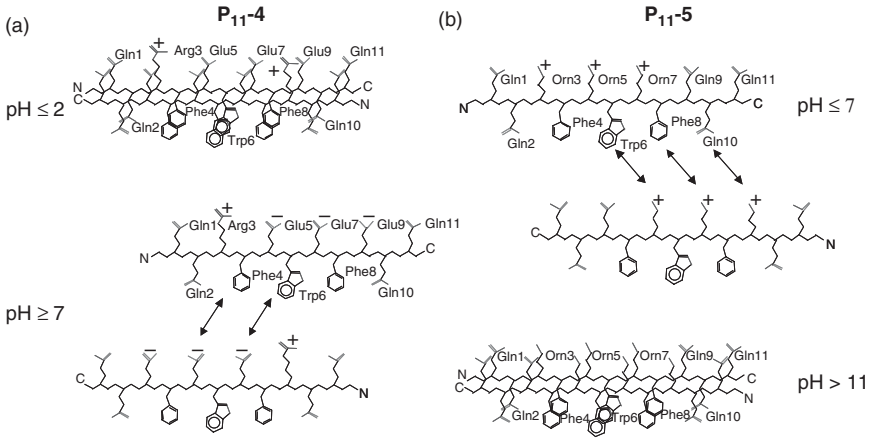

Figure 7 Self-assembly of (a) P_{11}-4 and (b) P_{11}-5 peptides at low and high pH values showing organization in dimeric tape-like substructures and monomeric states (Aggeli et al., 2003a, b).

pH behavior (Figure 7). In these two peptides, the interpeptide association energies, such as ε_{tape}, are strongly influenced by direct electrostatic forces between γ-COO^- in Glu^- or δ-NH_3^+ in Orn^+, respectively. This is illustrated by the acid–base titrations of fibrillar dispersions, which reveal that the deprotonation of the γ-COOH of Glu or of the δ-NH_3^+ of Orn^+ occurs over wide bands of up to 5 pH units, a feature of polyelectrolytes. The values of the energy parameters controlling self-assembly and the values of the critical concentration for self-assembly can therefore be smoothly and continuously varied by changing pH. This enables fast isotropic fluid-to-nematic and fluid-to-gel transitions to be triggered by relatively small additions of acid or base, typically one part in 10^3 by volume of 1 M HCl or NaOH, corresponding to a change of pH by a single unit (Figures 8 and 9).

A number of other pH-responsive β-sheet self-assembling peptides have also been described (Hong et al., 2003; Schneider et al., 2002; Zimenkov et al., 2006). One such class of peptides is EAK16, which includes a repetitive sequence of hydrophobic alanine and charged residues of glutamic acid and lysine (AEAEAKAKAEAEAKAK) (Zhang et al., 1993). The arrangement of the individual amino acids gives rise to two distinct faces: a hydrophobic side comprising solely alanines, and a charged side, of negative glutamic acid residues and positive lysine residues. This motif resulted in the rational design of a class of EKA16 peptides that could respond to a host of external environmental triggers. EAK16 IV (AEAEAEAEAKAKAKAK) is a variant of EAK16 II (AEAEAKAKAEAEAKAK). The subtle change to the peptide primary structure demonstrates vast differences in responsiveness to varying pH when

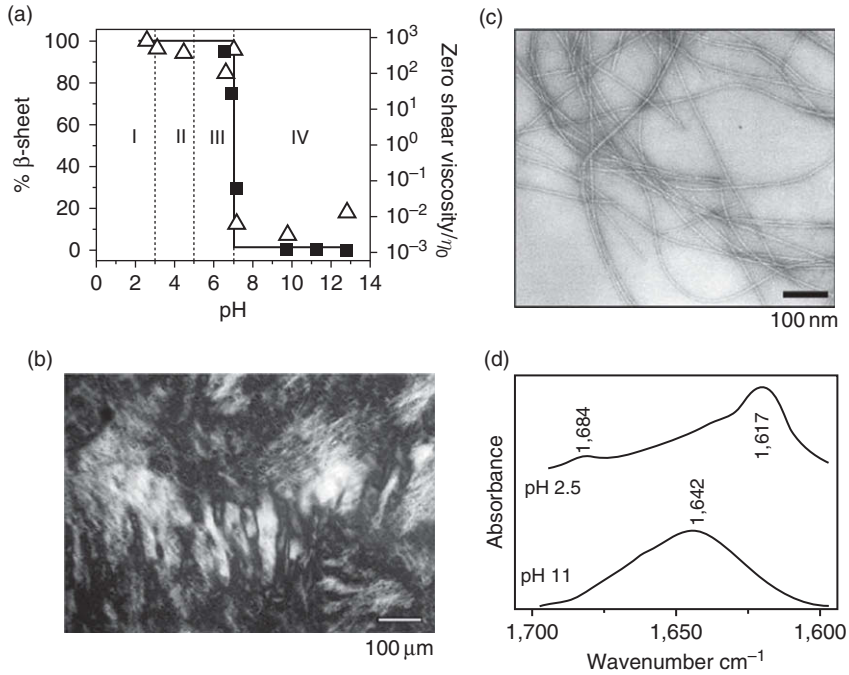

Figure 8 (a) Phase behavior of P_{11}-4 at $c = 6.3$ mM, as a function of pH in water: (I) nematic gel, (II) flocculate, (III) nematic fluid, (IV) isotropic fluid. The continuous line denotes the proportion of peptide in fibrils. (b) Polarizing optical micrograph of a P_{11}-4 gel in water ($c = 6.3$ mM, pH 3) showing a typical thick thread-like viscoelastic nematic texture (path length = 0.2 mm). (c) Transmission electron micrograph of a P_{11}-4 gel in water ($c = 6.3$ mM, pH = 3) showing semirigid fibrils and fibers. (d) FTIR spectrum of amide I′ bands showing β-sheet conformation of P_{11}-4 nematic gel ($c = 6.3$ mM) at pH 2.5 and random coil state of P_{11}-4 isotropic fluid ($c = 6.3$ mM) at pH 11 (Aggeli et al., 2003a, b).

compared to EAK II. Observations on the change in morphology were considered by Hong et al. (2003), and it was reported that the original EAK16 II motif showed no change in its morphology between the range of $4.0 < \text{pH} < 11$. However, the morphology of the EAK16 IV aggregates did depend on its environment. In a pH range of between 6.5 and 7.5, globular assemblies were observed. Below a pH of 6.5 and above a pH of 7.5, the structural morphology had changed to a fibrilar state (Hong et al., 2003). The slight difference in charge distribution is the reason for the observed behavior. In neutral conditions, EAK16 IV does not form nanostructures, this can be attributed to all of the ionizable side groups carrying their respective charge, and thus the electrostatic interactions produce a repulsive effect. When one side chain has become electrostatically neutral, this induced a conformational change.

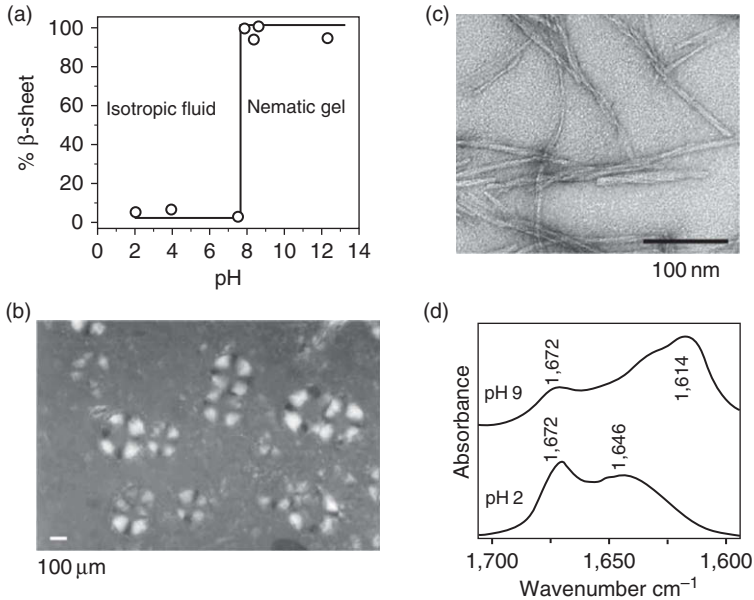

Figure 9 (a) Phase behavior of P_{11}-5 ($c = 13.1$ mM in water) as a function of pH, showing the sharp transition from isotropic fluid to nematic gel states at pH 7.5. (b) Polarizing optical micrograph showing nematic droplets with a radial director distribution (maltese cross) dispersed in an isotropic fluid phase. (c) Transmission electron micrograph of a gel (pH 9, $c = 13.1$ mM) showing semirigid fibrils. (d) FTIR spectrum of amide I′ bands showing β-sheet conformation of P_{11}-5 in the nematic gel state ($c = 13.1$ mM, pH 9), and the random coil conformation in the isotropic fluid state ($c = 13.1$ mM, pH 2) (Aggeli et al., 2003).

3.2. Ionic strength

The control on peptide self-assembly and material properties exerted by electrostatic interactions naturally leads to the question of how the self-assembly would be affected by another related chemical trigger, that is, changes in the ionic strength in solution. An increase in salt concentration in water would be expected to shield the electrostatic forces between side chains, change the magnitudes of energetic parameters, and shift both the critical concentration required for the onset of self-assembly and the observed pH of the transition from gel to fluid. A previous experimental study has revealed the influence of biologically relevant ionic strength on the self-assembly and gelation of pH responsive, systematically varied β-sheet tape-forming peptides, such as P_{11}-4 (Carrick et al., 2007). Another example is peptide P_{11}-9 ($CH_3CO—SSR^+FE^-WE^-FE^-SS—NH_2$), a variant of P_{11}-4. In order to assess the effect of addition of salt, first the self-assembling properties of P_{11}-9 in water in the absence of salt were established. P_{11}-9 ($c = 7.0$ mM) forms clear self-supporting gels at $pD \leq 3.2 \pm 0.2$ in D_2O (Figure 10a). FTIR spectra of the

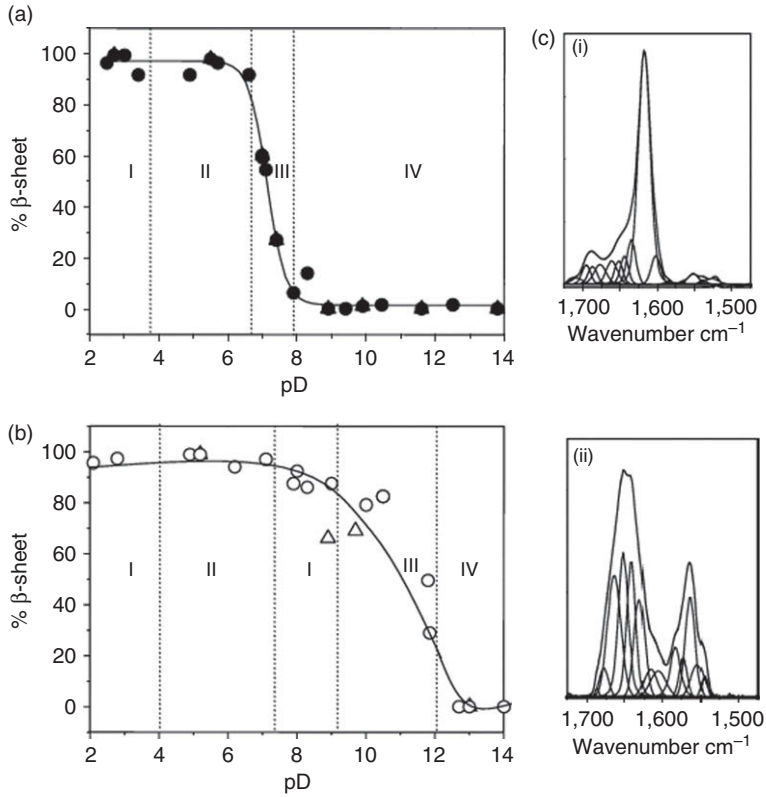

Figure 10 Self-assembly behavior of P_{11}-9 ($c = 7.0$ mM). (a) Percentage β-sheet of P_{11}-9 as a function of pD in D_2O. (b) Percentage β-sheet of P_{11}-9 in 130 mM NaCl in D_2O: (I) nematic gel, (II) flocculate, (III) nematic fluid, (IV) isotropic fluid. (c) FTIR absorption spectra of P_{11}-9: (i) nematic self-supporting gel at pD 2 in D_2O, (ii) monomeric isotropicfluid at pD 10 in D_2O (Carrick et al., 2007).

gels (Figure 10c(i)) have a large absorption band at 1,614 cm^{-1} corresponding to β-sheet aggregates and a weaker band at 1,684 cm^{-1} indicating an antiparallel β-sheet. In addition, a band at 1,710 cm^{-1} corresponding to COOD (protonated glutamic acid side chains) is observed. At $3.2 \leq pD \leq 6.8$, flocculates are obtained. The percentage of β-sheet within the flocculate is shown to be comparable to that in the self-supporting gels (Figure 10a), but the fibrillar aggregates are insoluble. At $pD \leq 3.2$, the gels have a single positive charge (arginine in position 3). Glutamic acid side chains begin to deprotonate as the pD is increased, and a situation where the peptide molecules have a net charge of 0 (+1 Arg, –1 Glu) will be encountered. Without sufficient repulsion between the fibrils, large insoluble aggregates are formed leading to flocculation. This explanation is evidenced by the disappearance of the very weak band at

1,710 cm^{-1} and the increase in a band at 1,565 cm^{-1} which corresponds to COO^- (i.e., deprotonated glutamic acid). At $6.8 \leq pD \leq 7.2$, clear viscous fluids are obtained as the peptide molecules begin to have a slight net negative charge and the fibrillar aggregates become soluble and establish gel networks. The FTIR spectra contain similar proportions of random coil (1,645 cm^{-1}) and β-sheet (1,614 cm^{-1}). At $pD > 7.2$, clear isotropic fluids are observed, accompanied by a characteristic random coil band at 1,645 cm^{-1}. As may be expected from the similarities of the primary structures, the pH-responsive behavior of P_{11}-9 is similar to that of P_{11}-4 (Figure 8). Addition of 130 mM NaCl shifts the beta-sheet to random coil transition by more than 3 units to higher pH (Figure 10b) and makes the transition broader compared to that in the absence of salt. The gels of P_{11}-9 at $pD \leq 3$ are shown by electron microscopy to be composed predominantly of micrometer-length fibrils, which are typically 5–7 nm at their widest point and 4 nm at their narrowest point (Figure 11). A twist pitch of

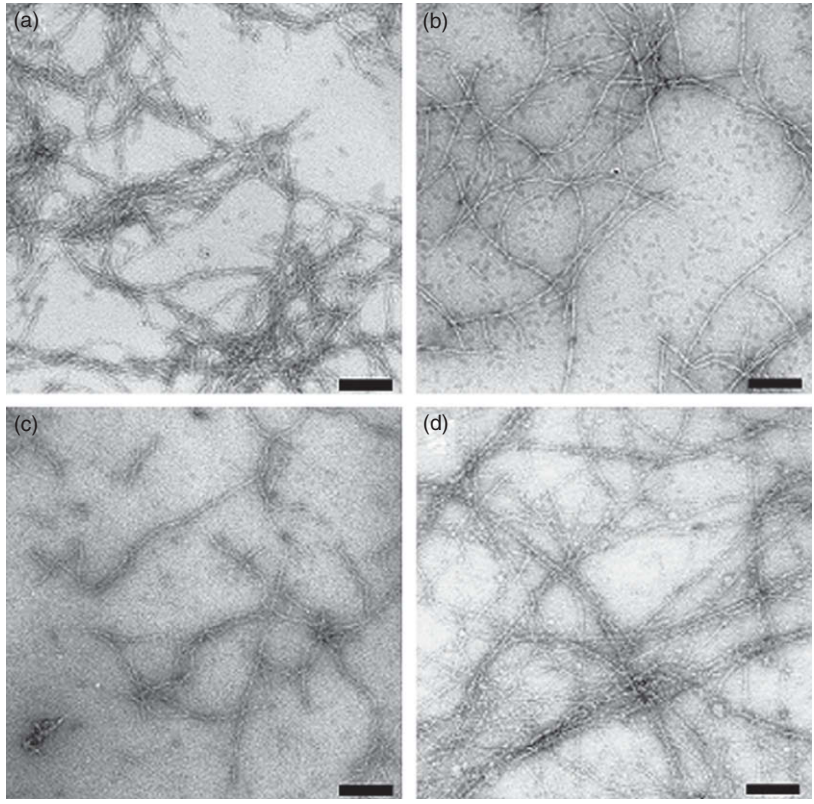

Figure 11 TEM of P_{11}-9 ($c = 7.0$ mM): (a) nematic gel at pD 2 in D_2O, (b) viscous fluid at pD 7 in D_2O, (c) weak gel of P_{11}-9 at $pD \sim 3$ in 130 mM NaCl in D_2O, (d) nematic gel at $pD \sim 8$ in 130 mM NaCl in D_2O. Scale bars 100 nm (Carrick et al., 2007).

50–80 nm is observed. Most fibrils are composed of two thinner structures, 2–4 nm in width. Flocculates at $3.2 \leq pD \leq 6.8$ and nematic fluids at $6.8 \leq pD \leq 7.2$ also contain fibrils of the 5–10 nm in width and micrometers in length.

In summary, aqueous solutions (~7 mM, equivalent to ~0.7% v/v) of amphiphilic β-sheet tape-forming peptides containing glutamic acid side chains are found to undergo significant changes as a function of pD (2–14) and salt concentration, depending on the deprotonation state of the side chains. Insoluble flocculates of self-assembling fibrils are observed when the net peptide charge is close to zero, nematic gels when there is a small amount of net charge, and monomeric fluid when there is a high net charge per peptide (–2 for solutions with no added salt and –3 for solutions with 130 mM added NaCl). In the absence of added salt, a sharp transition at $6.5 < pD < 8$ is observed from the antiparallel β-sheet at $pD < 6.5$ to the monomeric random coil at $pD > 8$. This is accompanied by a change of the solution properties from a nematic solution at $pD < 8$ to isotropic Newtonian fluid at $pD > 8$. The transition is reversible several times by cycling the pD up and down. In the presence of 130 mM NaCl, the transition becomes broader and shifts to higher pD, by 2–3 pD units. In this way, at physiological-like conditions (pD ~ 7–8, 130 mM NaCl), self-supporting nematic gels are now obtained rather than fluids. The shift of the transition to higher pD in the presence of added salt is attributed to screening of electrostatic repulsion between negative charges, as expected from the Derjaguin, Landau, Verwey, Overbeek (DLVO) theory (Carrick et al., 2007), rather than to a change in the pKa of glutamic acid residues in the presence of the added salt.

Peptide P_{11}-12 ($CH_3COSSR^+FO^+WO^+FE^-SSNH_2$) is similar to P_{11}-9 but is designed through the incorporation of ornithine side chains in positions 5 and 7 to have the opposite pH-responsive behavior to P_{11}-9. Solutions of P_{11}-12 at $pD < 9$ have an absorption band at 1,645 cm^{-1} corresponding to peptide in a random coil state. The large absorption band at 1,673 cm^{-1} corresponds to trifluoroacetic acid counterions (Figure 12a). Bands centered at 1,614 and 1,625 cm^{-1} were assigned to peptide in a β-sheet conformation and were seen to increase in magnitude as a function of pD. The weak absorption bands at 1,695 and 1,685 cm^{-1} indicate an antiparallel arrangement. In the range $9.5 < pD < 11.5$, the amount of β-sheet present is nearly 100%. However, at $pD > 11.5$, it starts dropping again. This may be explained by the increased presence of negatively charged carbamates and glutamic acid side chains and the loss of the positive charge on the arginine at $pD > 12.5$. This makes the net peptide charge higher than −1 and partially destabilizes the aggregates at very high pD. Addition of salt causes the conformation transition to shift by 2 pD units to lower pD (Figure 12b). In the absence of added salt at $pD \leq 8$ in D_2O, fibrils of

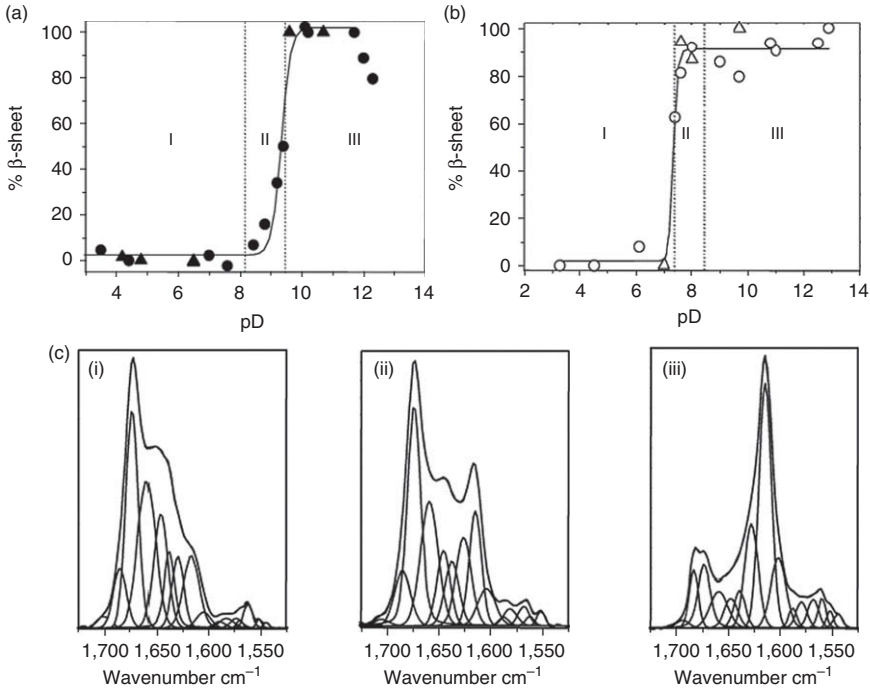

Figure 12 Self-assembly of P_{11}-12 at $c = 7.1$ mM. (a) Percentage β-sheet of P_{11}-12 as a function of pD in D_2O. (b) Percentage β-sheet of P_{11}-12 as a function of pD in 130 mM NaCl in D_2O: (I) isotropic fluid, (II) weakly nematic viscous fluid, (III) weakly nematic gel. (c) FTIR absorption spectra of P_{11}-12 in D_2O showing (i) monomeric peptide at pD 7, (ii) a viscous fluid at pD 9, (iii) a self-supporting gel at pD 10 (Carrick et al., 2007).

P_{11}-12 are not observed. At $8.5 \leq pD \leq 12$, fibrils and bundles composed of 3- to 4-nm wide fibrils are observed (Figure 13), which are similar to those observed for P_{11}-9 (Figure 11).

In summary, amphiphilic tape-forming peptides containing positively charged side chains are found to undergo major charges as a function of pD (2–14) and salt concentration, depending on the deprotonation state of the side chains. In the absence of added salt, a sharp transition at $8 < pD < 10$ is observed from gels with antiparallel β-sheet structure at $pD > 10$ to fluid solutions with monomeric random coil peptides at $pD < 8$. In the presence of 130 mM NaCl, the transition shifts to lower pD by 2–3 pD units. In this way, at physiological-like conditions ($pD \sim 7$–8), viscous nematic fluids are now obtained which convert to self-supporting gels at higher peptide concentration. These data show that the charged peptide solutions are reminiscent of the behavior of polyelectrolyte molecules and complexes (Tsuchida and Abe, 1982).

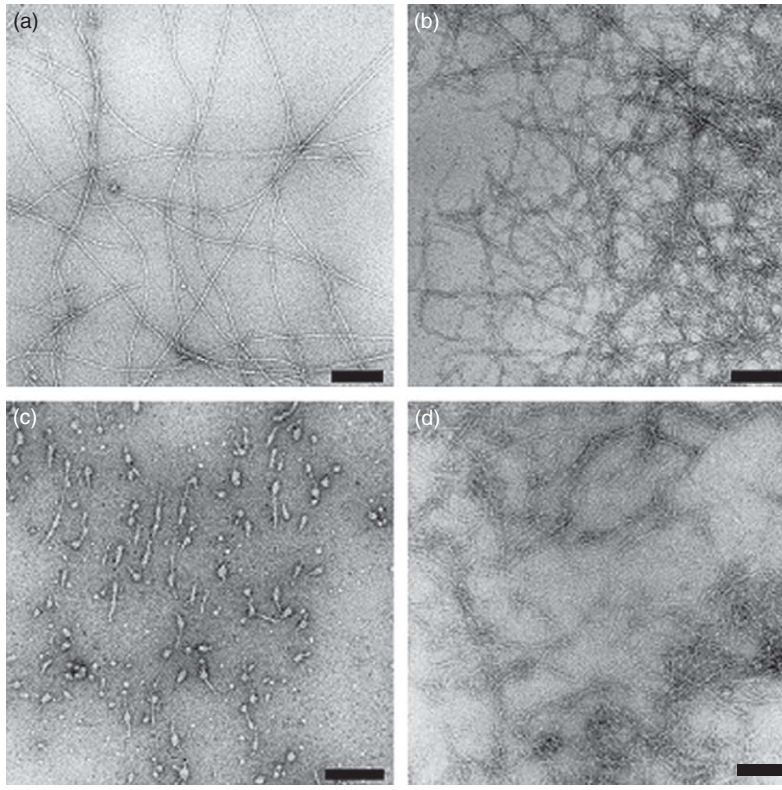

Figure 13 TEM of P_{11}-12 ($c = 7.1$ mM): (a) nematic fluid at pD 8.5 in D_2O, (b) nematic gel at pD 12 in D_2O, (c) isotropic fluid at pD 6 in 130 mM NaCl in D_2O, (d) nematic gel at pD 10 in 130 mM NaCl in D_2O. Scale bars 100 nm (Carrick et al., 2007).

Systematic studies of the morphology of the self-assembling fibrils by TEM revealed a surprising observation, namely that the most frequently observed fibrillar structures for a given peptide appear to be largely independent of ionic strength, phase (i.e., gel, flocculate, or nematic solution), and pD. In contrast, the characteristics of the fibrils seem to change significantly by modifications of the peptide primary structure and to a lesser extent by the presence of positively or negatively charged side chains.

These observations (Carrick et al., 2007) are also in line with data obtained with other families of gel-forming self-assembling peptides (Collier and Messersmith, 2003; Collier et al., 2001; Mart et al., 2006; Matsumura et al., 2006). Such a class of amphiphilic self-assembling peptides with complementary charges present on each molecule has been previously developed primarily for applications as 3D scaffolds for tissue engineering (Zhang et al., 1993). Aqueous gels formed by one such peptide, KFE12 (FKFEFK-FEFKFE), were stabilized in the presence of salts when the intermolecular

electrical double-layer repulsion became less than the van der Waals attraction. This is quantified by the DLVO theory, which predicts that addition of salts would screen charged groups from each other and would thus decrease the Debye length of the solvent (Caplan et al., 2000, 2002).

Another family of peptide amphiphiles consisting of a long hydrocarbon chain segment followed by a peptide segment has also been previously presented. Detailed studies of the rheological properties of aqueous solutions of a typical molecule PA-1 as a function of pH and a wide range of counter ions have been published (Stendahl et al., 2006). The data show that self-assembly of PA-1 and gelation are triggered by counterion screening and are in agreement with the DLVO theory. Another family of peptides designed to adopt a β-hairpin have also demonstrated a pH and ionic strength responsiveness (Schneider et al., 2002). An example of such a peptide is MAX1 ($VKVKVKV^{D}PPTKVKVKV—NH_2$). In a basic environment, the peptide adopts an amphiphilic β-hairpin conformation. One face of the hairpin is arranged with the hydrophobic valine and the opposing face is lined with hydrophilic lysine residues. Self-assembly of the individual monomeric hairpins occurs due to the formation of hydrogen bonds between discrete hairpins. At low pH, interstrand charged–charged repulsions between lysines destabilize individual hairpins and cause unfolding; subsequently this disrupts the conformation of the peptide in solution and results in total disassembly (Ozbas et al., 2004; Schneider et al., 2002). MAX 1 in an aqueous solution of pH ~ 7.4 required addition of 150 mM KF or 400 mM NaCl for self-assembly to occur.

3.3. Other

This section is by no means an exhaustive account of the various triggers used for self-assembly. It only serves as a quick reminder that apart from pH and ionic strength, which were discussed in the previous sections, a wide range of other factors may be used to control peptide self-assembly and gelation. For example, the ability of an enzyme to act as an external trigger to control self-assembly formation has been demonstrated in recent years (Mart et al., 2006; Ulijn, 2006). Enzyme-responsive self-assembling materials usually contain two main elements. The first is an enzyme-sensitive component which is essentially the trigger, and the second defines the higher order self-assembled structure through its intrinsic molecular characteristics (i.e., controls the weak noncovalent interactions that cause self-assembly) (Ulijn, 2006). A variant of spider dragline silk protein was amongst the first systems to demonstrate enzyme responsiveness. Here enzymatic dephosphorylation controlled the β-sheet formation of the protein (Winkler et al., 2000). The phosphorylation/dephosphorylation has also been used to trigger (Fmoc)-tyrosine into self-assembly. Fluid phosphorylated (Fmoc)-tyrosine was dephosphorylated by a phosphatase causing a phase transition from solution to a gel (Yang et al., 2006).

Another class of "switch" peptides has also been presented (Mutter et al., 2004). This work has developed further into a switchable peptidic material derived from the β-amyloid motif which has an enzymatic triggering system. Controlling the self-assembly of amyloid β-derived peptides by using enzyme-triggered intermolecular acyl migration to promote gel formation has been demonstrated. Modified serine, threonine, and cysteine had enzyme-removable acyl groups attached at the N-terminus which were also modified to have a linked peptide chain. Enzyme deacylation of the *N*-acyl group transferred the linked peptide chain to the amine terminus resulting in a conformation change into a β-sheet (Dos Santos et al., 2005). Consecutive switching of the peptide had been demonstrated and the conformation change was deemed to be spontaneous.

Thermal (Collier et al., 2001; Pochan et al., 2003) and phototriggering (Bosques and Imperiali, 2003; Collier et al., 2001) has also been demonstrated for gel-forming self-assembling peptides. For example, the incorporation of a photoactive compound within the primary structure of a β-hairpin facilitated the use of light to act as an external trigger. The covalent inclusion of a photocage (α-carboxy-2-nitrobenzyl) electrostatically prevented peptide folding, subsequently inhibiting self-assembly. Upon irradiation with ultraviolet light, the photocage was released and self-assembly was triggered (Haines et al., 2005).

3.4. Heteroaggregates formed by complementary peptides

An approach to change the magnitudes of the energetic parameters and greatly affect the tendency for self-assembly and the material properties, without changing the solution conditions, is to mix solutions of complementary peptides together. To demonstrate this principle, two such peptides C (cationic) and A (anionic) have been previously designed (Figure 14) (Aggeli et al., 2003a, b). The two complementary peptides C and A must have a propensity to antiparallel β-sheet formation, appropriate complementarity in the disposition of charged amino acid side chains, and at least one additional charged amino acid per peptide pair to stabilize the peptide fibrillar network against flocculation. Polyelectrolyte β-sheet complexes (PECs) were shown to form on mixing aqueous solutions of such cationic and anionic peptides (Figure 15a and b). This results in the spontaneous self-assembly of fibrillar networks (Figure 15d) and the production of nematic hydrogels (Figure 15c). These complexes have a 1:1 molar stoichiometry, and their networks are robust to variations in pH or peptide concentration. They may be likened to the PECs formed on mixing oppositely charged polymeric polyelectrolytes except that their supramolecular structures are quite different. In the case of peptide complexes, the fibrils have more definitive molecular and mesoscopic structures making it easier to specify the requisite molecular design. Another example of complementary self-assembling peptide amphiphiles was also reported (Niece et al., 2003).

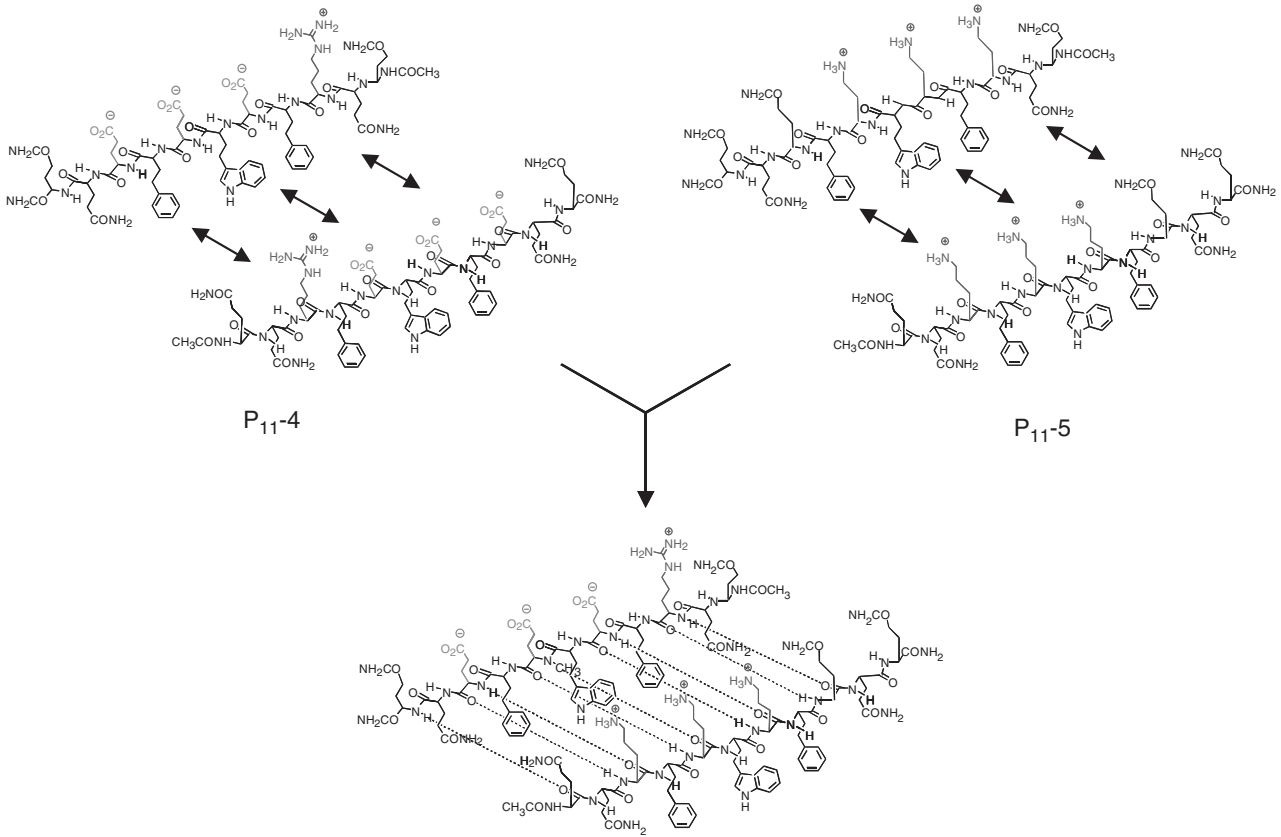

Figure 14 Molecular structures of P_{11}-4, P_{11}-5, and the complex showing the electrostatic charge distributions at pH 7.3 (Aggeli et al., 2003).

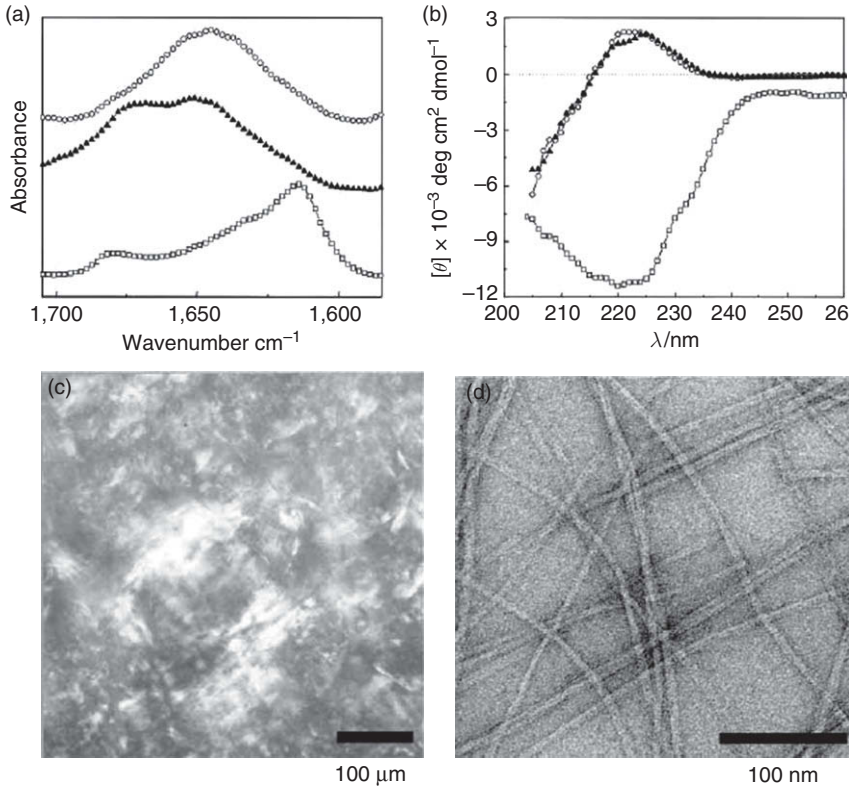

Figure 15 (a) FTIR spectra showing the initial random coil state of P_{11}-4 (○) and P_{11}-5 (▲) in 6.3 mM aqueous solutions at pH 7.3 prior to mixing, and the β-sheet conformation of the polyelectrolyte complex after mixing (□). (b) Far-UV CD spectra showing the initial random coil states of P_{11}-4 (○) and P_{11}-5 (▲) in aqueous solutions ($c = 3.1$ mM) prior to mixing, and the β-sheet complex formed after mixing (□). (c) Polarizing optical micrograph of the gel ($c = 6.3$ mM) formed after mixing aqueous solutions of the monomeric peptides at pH 7.3 showing a typical nematic gel texture. (d) Transmission electron micrograph showing mainly fibrils and a few fibers in the nematic gel ($c = 6.3$ mM) (Aggeli et al., 2003a, b).

4. PEPTIDE SELF-ASSEMBLY ON SURFACES

In order to achieve thorough fundamental understanding of biomolecular self-assembly, it is imperative to study 1D tape-like self-assembly not only in bulk solution but also at interfaces. An example of a biologically relevant interface is that of the lipid bilayer. Systematic peptide-lipid studies have begun to offer an insight into the basic principles and mechanisms of interactions of self-assembling peptides with model lipid layers (Protopapa et al., 2006).

Other studies of the tape-forming peptide P_{11}-2 have focused on its interaction with model solid surfaces, such as mica (Whitehouse et al., 2005). It was shown that the presence of the surface has a profound effect on peptide self-assembly. Monomeric peptides in solution below the critical concentration for solution self-assembly were found to interact with the mica surface via the charged amino acid residues Arg and Glu present on the polar side of the peptide and the corresponding negative charges and positively charged counterions on mica surface. Furthermore, adsorbed monomeric peptides went on to self-assemble on the solid surface producing individual tapes, with measured width of 4.9 nm and height of 0.8 nm in agreement with the molecular dimensions (Figure 16). Effectively, the solid surface acts as a template for the induction of peptide self-assembly at concentrations well below their critical concentration for self-assembly in solution. The tapes are stabilized by the intermolecular peptide interactions and also by the interactions of the polar face of the tape with the mica (Figure 17). The tapes on the surface are found to be completely flat, unlike their twisted counterparts in solution. The elastic penalty for untwisting the tape is thought to be compensated for by the gain in enthalpy due to tape–mica interactions. In order for the tapes to maximize their interaction with the surface, they don't overlap with one another, that is, as soon as they grow enough to meet another tape, tape growth stops. In this way, they

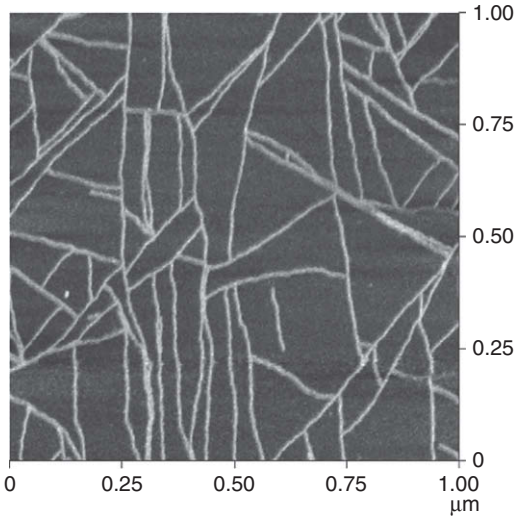

Figure 16 In situ AFM images of single β-sheet tapes grown on mica from 5 μM P_{11}-2 in 10% H_2O in 2-propanol. The tapes are aligned with the hexagonal symmetry of the underlying mica lattice (Whitehouse et al., 2005).

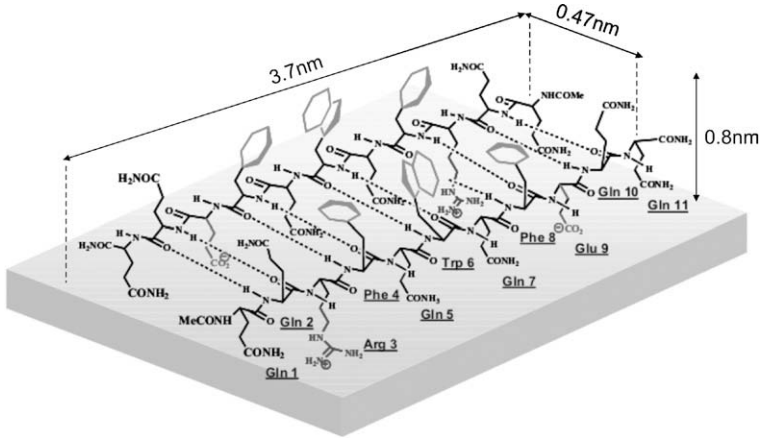

Figure 17 Schematic diagram showing the orientation and dimensions of a dimeric P_{11}-2 peptide tape when adsorbed at the surface of mica (Whitehouse et al., 2005).

form true single-molecule thick surface coatings. The macroscopic arrangement of the tapes on the surface can be controlled: hexagonal arrangement following the underlying mica crystal lattice, macroscopic alignment facilitated by shear field or side by side arrangement into tactoid structures depending on the drying process.

5. CONCLUSIONS AND FUTURE PROSPECTS

A theoretical framework exists that describes well 1D peptide tape self-assembly in solution in terms of a set of five molecular energetic parameters. However, it is currently not known how the magnitudes of the energetic parameters vary with changes of the peptide primary structure and solution conditions. Extensive systematic studies are underway to establish this quantitative information. The combined knowledge of the quantitative energetic parameters as a function of peptide chemistry and external condition, together with the mathematical model, can be a uniquely powerful tool at our disposal for understanding in detail biological self-assembly and for the efficient design of peptides and proteins with well-defined combination of self-assembling properties to fit appropriate applications.

For example, it will be possible to design peptides that aggregate in well-defined morphology, for example, fibrils of specific and controllable width and twist pitch to act as versatile templates for nanoporous inorganic materials (e.g., silica nanotubes) (Meegan et al., 2004). Another opportunity that opens up will be the ability to produce by precise molecular engineering, a

range of injectable self-assembling nanostructured networks with tunable activity, mechanical properties, and rates of dissolution to be used, for example, in health care (Bell et al., 2006; Firth et al., 2006; Kirkham et al., 2007; Scanlon et al., 2007) or screening devices. Similar theoretical and quantitative insight needs to be extended to peptide self-assembly on surfaces. This will allow us to produce ultrathin peptide nanocoatings on a variety of substrates, for example, for biomaterial or catalysis applications. The field of protein-like self-assembly is fairly new, but very promising and the opportunities it offers are limitless. The fundamental understanding of mechanisms and principles that drive protein-like self-assembly will become increasingly important as scientists will strive to come up with gradually more functional and complex protein-like building blocks for industrial applications.

REFERENCES

Aggeli, A., Bell, M., Boden, N., Carrick L.M., and Strong A.E. "Self-assembling peptide polyelectrolyte beta-sheet complexes form nematic hydrogels". *Angew. Chem. Int. Ed.* **42**(45), 5603–5606 (2003a).

Aggeli, A., Bell, M., Boden, N., Keen, J.N., Knowles, P.F., McLeish, T.C.B., Pitkeathly, M., and Radford S.E. "Responsive gels formed by the spontaneous self-assembly of peptides into polymeric beta-sheet tapes". *Nature* **386**(6622), 259–262 (1997a).

Aggeli, A., Bell, M., Boden, N., Keen, J.N., McLeish, T.C.B., Nyrkova, I., Radford, S.E., and Semenov, A. "Engineering of peptide beta-sheet nanotapes". *J. Mater. Chem.* **7**(7), 1135–1145 (1997b).

Aggeli, A., Bell, M., Carrick, L.M., Fishwick, C.W.G., Harding, R., Mawer, P.J., Radford, S.E., Strong A.E., and Boden, N. "pH as a trigger of peptide beta-sheet self-assembly and reversible switching between nematic and isotropic phases". *J. Am. Chem. Soc.* **125**(32), 9619–9628 (2003b).

Aggeli, A., Boden N., and Zhang S., "Self-Assembling Peptide Systems in Biology, Medicine and Engineering". Kluwer Academic Publishers, Dordrecht, The Netherlands (2001a).

Aggeli, A., Nyrkova, I.A., Bell, M., Harding, R., Carrick, L., McLeish, T.C.B., Semenov, A.N., and Boden, N. "Hierarchical self-assembly of chiral rod-like molecules as a model for peptide beta-sheet tapes, ribbons, fibrils, and fibers". *Proc. Nat. Acad. Sci. U.S.A.* **98**(21), 11857–11862 (2001b).

Bell, C.J., Carrick, L.M., Katta, J., Jin, Z.M., Ingham, E., Aggeli, A., Boden, N., Waigh T.A., and Fisher, J. "Self-assembling peptides as injectable lubricants for osteoarthritis". *J. Biomed. Mater. Res. Part A* **78A**(2), 236–246 (2006).

Bosques, C.J., and Imperiali B. "Photolytic control of peptide self-assembly". *J. Am. Chem. Soc.* **125**(25), 7530–7531 (2003).

Burkoth, T.S., Benzinger, T.L.S., Jones, D.N.M., Hallenga, K., Meredith, S.C., and Lynn D.G. "C-terminal PEG blocks the irreversible step in ß-amyloid (10–35) fibrillogenesis". *J. Am. Chem. Soc.* **120**(30), 7655–7656 (1998).

Caplan, M.R., Moore, P.N., Zhang, S.G., Kamm, R.D., and Lauffenburger, D.A. "Self-assembly of a beta-sheet protein governed by relief of electrostatic repulsion relative to van der Waals attraction". *Biomacromolecules* **1**(4), 627–631 (2000).

Caplan, M.R., Schwartzfarb, E.M., Zhang, S., Kamm, R.D., and Lauffenburger, D.A. "Control of self-assembling oligopeptide matrix formation through systematic variation of amino acid sequence". *Biomaterials* **23**(1), 219–227 (2002).

Carrick, L.M., Aggeli, A., Boden, N., Fisher, J., Ingham, E., and Waigh, T.A. "Effect of ionic strength on the self-assembly, morphology and gelation of pH responsive beta-sheet tape-forming peptides". *Tetrahedron* **63**(31), 7457–7467 (2007).

Chothia, C. "Conformation of twisted beta-pleated sheets in proteins". *J. Mol. Biol.* **75**(2), 295–302 (1973).

Collier, J.H., Hu, B.H., Ruberti, J.W., Zhang, J., Shum, P., Thompson, D.H., and Messersmith, P.B. "Thermally and photochemically triggered self-assembly of peptide hydrogels". *J. Am. Chem. Soc.* **123**(38), 9463–9464 (2001).

Collier, J.H., and Messersmith, P.B. "Enzymatic modification of self-assembled peptide structures with tissue transglutaminase". *Bioconjugate Chem.* **14**(4), 748–755 (2003).

de Loos, M., van Esch, J., Kellogg, R.M., and Feringa, B.L. "Chiral recognition in bis-urea-based aggregates and organogels through cooperative interactions". *Angew. Chem. Int. Ed.* **40**(3), 613–616 (2001).

Dobb, M.G., Johnson, D.J., and Saville, B.P. "Supramolecular structure of a high-modulus polyaromatic fiber (Kevlar 49)". *J. Polym. Sci. Part B-Polym. Phys.* **15**(12), 2201–2211 (1977).

Dos Santos, S., Chandravarkar, A., Mandal, B., Mimna, R., Murat, K., Saucede, L., Tella, P., Tuchscherer, G., and Mutter, M. "Switch-peptides: Controlling self-assembly of amyloid beta-derived peptides in vitro by consecutive triggering of acyl migrations". *J. Am. Chem. Soc.* **127**(34), 11888–11889 (2005).

Firth, A., Aggeli, A., Burke, J.L., Yang, X.B., and Kirkham, J. "Biomimetic self-assembling peptides as injectable scaffolds for hard tissue engineering". *Nanomedicine* **1**(2), 189–199 (2006).

Gronwald, O., Snip, E., and Shinkai, S. "Gelators for organic liquids based on self-assembly: a new facet of supramolecular and combinatorial chemistry". *Curr. Opin. Colloid Interface Sci.* **7**(1–2), 148–156 (2002).

Haines, L.A., Rajagopal, K., Ozbas, B., Salick, D.A., Pochan, D.J., and Schneider, J.P. "Light-activated hydrogel formation via the triggered folding and self-assembly of a designed peptide". *J. Am. Chem. Soc.* **127**(48), 17025–17029 (2005).

Hanabusa, K., Yamada, M., Kimura, M., and Shirai, H. "Prominent gelation and chiral aggregation of alkylamides derived from trans-1,2-diaminocyclohexane". *Angew. Chem. Int. Ed.* **35**(17), 1949–1951 (1996).

Hong, Y., Legge, R.L., Zhang, S., and Chen, P. "Effect of amino acid sequence and pH on nanofiber formation of self-assembling peptides EAK16-II and EAK16-IV". *Biomacromolecules* **4**(5), 1433–1442 (2003).

Kirkham, J., Firth, A., Vernals, D., Boden, N., Robinson, C., Shore, R.C., Brookes, S.J., and Aggeli, A. "Self-assembling peptide scaffolds promote enamel remineralization". *J. Dental Res.* **86**(5), 426–430 (2007).

Lashuel, H.A., LaBrenz, S.R., Woo, L., Serpell, L.C., and Kelly, J.W. "Protofilaments, filaments, ribbons, and fibrils from peptidomimetic self-assembly: Implications for amyloid fibril formation and materials science". *J. Am. Chem. Soc.* **122**(22), 5262–5277 (2000).

Manning, M.C., Illangasekare, M., and Woody, R.W. "Circular-dichroism studies of distorted alpha-helices, twisted beta-sheets, and beta-turns". *Biophys. Chem.* **31**(1–2), 77–86 (1988).

Marini, D.M., Hwang, W., Lauffenburger, D.A., Zhang, S.G., and Kamm, R.D. "Left-handed helical ribbon intermediates in the self-assembly of a beta-sheet peptide". *Nano Lett.* **2**(4), 295–299 (2002).

Mart, R.J., Osborne, R.D., Stevens, M.M., and Ulijn, R.V. "Peptide-based stimuli-responsive biomaterials". *Soft Matter* **2**(10), 822–835 (2006).

Matsumura, S., Uemura, S., and Mihara, H. "Metal-triggered nanofiber formation of His-containing beta-sheet peptide". *Supramol. Chem.* **18**(5), 397–403 (2006).

Meegan, J.E., Aggeli, A., Boden, N., Brydson, R., Brown, A.P., Carrick, L., Brough, A.R., Hussain, A., and Ansell, R.J. "Designed self-assembled beta-sheet peptide fibrils as templates for silica nanotubes". *Adv. Funct. Mater.* **14**(1), 31–37 (2004).

Mutter, M., Chandravarkar, A., Boyat, C., Lopez, J., Dos Santos, S., Mandal, B., Mimna, R., Murat, K., Patiny, L., and Saucede, L. "Switch peptides in statu nascendi: induction of conformational transitions relevant to degenerative diseases". *Angew. Chem. Int. Ed.* **43**(32), 4172–4178 (2004).

Niece, K.L., Hartgerink, J.D., Donners, J.J.J.M., and Stupp, S.I. "Self-assembly combining two bioactive peptide-amphiphile molecules into nanofibers by electrostatic attraction". *J. Am. Chem. Soc.* **125**(24), 7146–7147 (2003).

Nyrkova, I.A., Semenov, A.N., Aggeli, A., Bell, M., Boden, N., and McLeish, T.C.B. "Self-assembly and structure transformations in living polymers forming fibrils". *Eur. Phys. J. B* **17**(3), 499–513 (2000a).

Nyrkova, I.A., Semenov, A.N., Aggeli, A., and Boden, N. "Fibril stability in solutions of twisted beta-sheet peptides: a new kind of micellization in chiral systems". *Eur. Phys. J. B* **17**(3), 481–497 (2000b).

Ozbas, B., Rajagopal, K., Schneider, J.P., and Pochan, D.J. "Semiflexible chain networks formed via self-assembly of ß-hairpin molecules". *Phys. Rev. Lett.* **93**(26), 268106 (2004).

Perutz, M.F., Johnson, T., Suzuki, M., and Finch, J.T. "Glutamine repeats as polar zippers – their possible role in inherited neurodegenerative diseases". *Proc. Nat. Acad. Sci. U.S.A.* **91**(12), 5355–5358 (1994).

Pochan, D.J., Schneider, J.P., Kretsinger, J., Ozbas, B., Rajagopal, K., and Haines, L. "Thermally reversible hydrogels via intramolecular folding and consequent self-assembly of a de Novo designed peptide". *J. Am. Chem. Soc.* **125**(39), 11802–11803 (2003).

Protopapa, E., Aggeli, A., Boden, N., Knowles, P.F., Salay, L.C., and Nelson, A. "Electrochemical screening of self-assembling beta-sheet peptides using supported phospholipid monolayers". *Med. Eng. Phys.* **28**(10), 944–955 (2006).

Qu, Y., Payne, S.C., Apkarian, R.P., and Conticello, V.P. "Self-assembly of a polypeptide multi-block copolymer modeled on dragline silk proteins". *J. Am. Chem. Soc.* **122**, 5014 (2000).

Scanlon, S., Aggeli, A., Boden, N., Koopmans, R.J., Brydson, R., and Rayner, C.M., "Peptide aerogels comprising self-assembling nanofibrils". *Micro Nano Lett.* **2**, 24–29 (2007).

Schneider, J.P., Pochan, D.J., Ozbas, B., Rajagopal, K., Pakstis, L., and Kretsinger, J. "Responsive hydrogels from the intramolecular folding and self-assembly of a designed peptide". *J.Am. Chem. Soc.* **124**(50), 15030–15037 (2002).

Semenov, A.N., and Khokhlov, A.R. "Statistical physics of liquid-crystalline polymers". *Physics-Uspekhi* **31**(11), 988–1014 (1988).

Stendahl, J.C., Rao, M.S., Guler, M.O., and Stupp, S.I. "Intermolecular forces in the self-assembly of peptide amphiphile nanofibers". *Adv. Funct. Mater.* **16**(4), 499–508 (2006).

Terech, P., and Weiss, R.G. "Low molecular mass gelators of organic liquids and the properties of their gels". *Chem. Rev.* **97**(8), 3133–3159 (1997).

Tsuchida, E., and Abe, K. "Interactions between macromolecules in solution and intermacromolecular complexes". *Adv. Polym. Sci.* **45**, 1–119 (1982).

Ulijn, R.V. "Enzyme-responsive materials: a new class of smart biomaterials". *J. Mater. Chem.* **16**(23), 2217–2225 (2006).

Weiss, R.G., and Terech, P. "Molecular Gels: Materials with Self-Assembled Fibrillar Networks". Springer, Dordrecht, , The Netherlands (2006).

Whitehouse, C., Fang, J.Y., Aggeli, A., Bell, M., Brydson, R., Fishwick, C.W.G., Henderson, J.R., Knobler, C.M., Owens, R.W., Thomson, N.H., Smith, D.A., and Boden, N. "Adsorption and self-assembly of peptides on mica substrates". *Angew. Chem. Int. Ed.* **44**(13), 1965–1968 (2005).

Wilson, M., Kannangara, K., Smith, G., and Simmons, M. "Nanotechnology: Basic Science and Emerging Technologies". CRC Press, Sydney, Australia (2002).

Winkler, S., Wilson, D., and Kaplan, D.L. "Controlling beta-sheet assembly in genetically engineered silk by enzymatic phosphorylation/dephosphorylation". *Biochemistry* **39**(41), 12739–12746 (2000).

Yamada, N., Ariga, K., Naito, M., Matsubara, K., and Koyama, E. "Regulation of beta-sheet structures within amyloid-like beta-sheet assemblage from tripeptide derivatives". *J. Am. Chem. Soc.* **120**(47), 12192–12199 (1998).

Yang, Z., Liang, G., Wang, L., and Xu, B. "Using a kinase/phosphatase switch to regulate a supramolecular hydrogel and forming the supramolecular hydrogel in vivo". *J. Am. Chem. Soc.* **128**(9), 3038–3043 (2006).

Zhang, S.G., Holmes, T., Lockshin, C., and Rich, A. "Spontaneous assembly of a self-complementary oligopeptide to form a stable macroscopic membrane". *Proc. Nat. Acad. Sci. U.S.A.* **90**(8), 3334–3338 (1993).

Zimenkov, Y., Dublin, S.N., Ni, R., Tu, R.S., Breedveld, V., Apkarian, R.P., and Conticello, V.P. "Rational design of a reversible pH-responsive switch for peptide self-assembly". *J. Am. Chem. Soc.* **128**(21), 6770–6771 (2006).